

ORIGINAL ARTICLE

Open Access



Seismic waves of the 10 December 2020 M6.6 Yilan earthquake observed by interferometric fiber-optic gyroscope

Hung-Pin Chung^{1,2,3}, Sheng-Han Chang¹, Ching-Lu Hsieh¹, Hsuan Yang³, Chii-Chang Chen², Jann-Yenq Liu^{1,4,5}, Horng-Yuan Yen⁶ and Yen-Hung Chen^{1,2*}

Abstract

A newly developed cost-effective fiber-optic gyroscope (FOG) and an existing seismometer co-locating at the campus of National Central University (NCU) recorded seismic waves of a M6.6 Yilan earthquake and aftershock events occurring at around 24.74° N 122.03° E (88 km away from NCU) during 10–11 December 2020. Two nearest accessible broadband seismographs located in Hsinchu have also been employed as measurement references for facilitating the analysis of the detected seismic signals. Conventional seismometers usually detect the translational components of the seismic waves, while the FOG observes the rotational component. The recorded FOG data exhibit high-resolution details of the rotational component of shockwaves, which provides additional information of seismic waves. The shock waveforms of the translational and rotational components, analyzed under the conservation of the shock wave energy density received by FOG and seismograph, are found to be significantly correlated. The correlation coefficients of 60-s data are > 0.85 for the main shock and > 0.86 for the aftershock, while those of the 10-s peak periods are as high as 0.9064 and 0.8953, respectively. The highly correlated data imply that the energy registered by the two devices are equivalent. The optical interference-based rotation sensor of the cost-effective FOG provides a high sensitivity of better than 3.6 deg/h and an extended dynamic sensing range as high as 55 dB with the fully sensing ability from ± 3.6 deg/h to $\pm 720,000$ deg/h. The FOG seismometer sheds some light on building an earthquake six-degree-of-freedom observation array to have a bettering on the understanding of the seismicity.

Key Points

1. A NCU fiber-optic gyroscopy station detects the earthquake rotational motion.
2. The bias stability of the fiber-optic gyroscope reaches 0.034 deg/h.
3. The correlation of translational and rotational shockwave components is > 0.85 .

Keywords: Fiber-optic gyroscope, Rotational seismology, Seismic sensor

1 Introduction

Taiwan is on the Pacific Rim Seismic Belt and surrounded by the ocean and located in the subduction zone between the Philippine-Sea and Eurasian plates. This geographically special intersection makes the region surrounding Taiwan a seismically active zone, a well-known world's

*Correspondence: yhchen@dop.ncu.edu.tw

¹ Center for Astronautical Physics and Engineering, National Central University, Taoyuan City, Taiwan
Full list of author information is available at the end of the article

best laboratory for studying seismology. At present, Taiwan's seismic observation facilities, including the quick report system, strong earthquake observation network, early warning system, and the "Broadband Array in Taiwan for Seismology (BATS)" (operated by the Institute of Earth Sciences, Academia Sinica), record most of the displacement, velocity, and acceleration information of the earth's surface caused by earthquake events in the respectively covered districts. However, a certain amount of the seismic energy is transmitted by rotational components. Gyroscopes are possible to record the rotation information of the seismic waves with high fidelity, which makes up the seismic sensing data with additional information of the three rotational components to fully map out the six degrees of freedom of moving objects and therefore, to facilitate the complete reconstruction and description of the seismic waves.

The common seismographs can be divided into several types, such as broadband seismographs (Lough 2014), mid-to-long-period seismographs (Warner 2014), and acceleration sensors (Van Hees et al. 2009), which are used to record/derive the shockwave velocity, frequency, and acceleration values in 3 translational axes. In NCU campus, we have a fixed seismograph station equipped with several seismometers including an acceleration-type strong motion recorder (SMART 24A) and a broadband seismograph (KS-200BH). Various portable seismometers like CMG-6TD broadband seismographs, SAMTAC-801B recorders, and VSE-311C sensors for mid-to-long period recording, and a K2 digital acceleration seismic recording system can also be found in individual laboratories at NCU. However, the main observation information obtained from the above-mentioned sensors is the linear velocity or linear acceleration data, which are associated with the translational components of shockwaves. To fully describe the dynamics of a moving object, as the inertial measurement unit does in the inertial navigation field, we need the 6 degree-of-freedom data collected from the 3-axis rotational components and 3-axis translational components of motions. To obtain the missing rotation information, the gyroscopes are usually needed. The origin of measuring earthquakes with gyroscopes can be traced back to 1979 (Kurosu et al. 1979), and a review paper in 2016 suggests that the gyroscopes can open the new era of seismic monitoring, especially using the fiber-optic gyroscope (FOG) to monitor the near-field earthquake activities (Velikoseltsev et al. 2012). There were many earthquakes recorded by gyroscopes in this decade, including the earthquake rotational motions recorded by ring-laser gyroscopes (RLG) for far-field earthquakes in Italy during 2016–2021 (Simonelli et al. 2018; Simonelli et al. 2021). To make up the missing rotation information of seismic waves, since 2008, the rotation seismology has

attracted the attention of geophysicists in Taiwan (Lin et al. 2009; Lee et al. 2009), and FOG-based rotational sensors (iXBlue blueseis-3A) have been deployed as a Nanao array situated in east of Taiwan to construct a six degree-of-freedom broadband ground-motion observational network (Yuan et al. 2020). However, the use of optic-based gyroscopes to measure seismic information is currently relatively scarce and much expensive. To address this issue, we have developed at National Central University (NCU), Taiwan a cost-effective FOG-based seismic sensor via the use of a fully homemade, compact FOG with a remodeled configuration redesigned from a conventional FOG. In this study, we demonstrate the developed FOG is capable of the detection of an ultra-slow rotation motion with a sensitivity better than 3.6 deg/h, with which we have successfully detected the rotational components of shockwaves from the M6.6 Yilan earthquake and aftershock events which is 88 km away from NCU on 10–11 December 2020.

2 The fiber-optic gyroscope

Gyroscopes are usually used for monitoring the orientation and angular velocity of a moving object like vehicles and drones in general applications. The practical and market-proven gyroscopes include the microelectromechanical-system (MEMS) gyroscopes, FOG, RLG, and mechanical gyroscopes, developed for different applications. The key specification of gyroscopes is the accuracy of the angular velocity, which can be defined by the parameters of the bias stability and the angular random walk (ARW). The bias stability is an important index of gyroscope performance, which is also used to define the gyroscope grades as the consumer grade (>100 – $10,000$ deg/h), the industrial and space grade (0.1 – 100 deg/h), the tactical grade (0.01 – 0.1 deg/h), and the strategic grade (<0.001 deg/h). Another important performance index of gyroscope is the scale factor linearity, which is defined by the scale factor variation in the full sensing dynamic range. The scale factor is a coefficient translating the angular rate of the test object to the device digital output in a linear scaling law. The consumer grade gyroscopes feature lower cost and have been applied to such as the smartphones, robotics, quadcopters, gamepad, and virtual reality helmets thanks to the great mass production capacity of the semiconductor industry. The MEMS gyroscopes has already oligopolized this consumer market (Fact 2021). However, based on the optical interference, the FOG and RLG are time-tested solutions for the industrial grade, tactical grade, and military strategy grade applications.

Through the Sagnac effect (Arditty and Lefevre 1981), by monitoring the phase and intensity changes of the optical interference signal, one can convert different

observed physical quantities to optical domain information, with different modulation and demodulation schemes. Based on this effect, FOGs use highly sensitive optical interference to sense the angular velocity of a moving object via measuring the phase differences between the optical waves propagating clockwise and counter-clockwise in an optical fiber coil during the movement. The FOG sensitivity is a function of the structural parameters of the sensing coil, which in principle makes it relatively simple to adjust for a desired grade for different applications. It is worth mentioning that a low-to-mid grade FOG (0.1–10 deg/h) has shown the capability of performing the near-field seismic sensing (Lee et al. 2012). Most recently, 3-axis FOG-based rotational seismometers have been demonstrated in 2021 (Cao et al. 2021).

In this work, we developed a cost-effective seismic sensor based on a fully homemade, compact FOG with a simplified control logic circuit via open-loop and

closed-loop control approaches. The rotation rate of the FOG is characterized by a test on a single-axis reference rotating stage having a dynamic range from -200 to $+200$ deg/s. Figure 1a shows the physical picture of the sensor (NCU-FOG). The FOG sensor unit is mounted on a granite anti-vibration platform for conducting a steady and long-term monitoring experiment with its azimuth being approximately aligned with the NS direction. The normal axis of the FOG is roughly perpendicular to the earth surface. The stability of a FOG can be characterized by the Allan deviation analysis (Lefevre 2014) which gives the information of the long-term bias stability and the short-term noise indexed by the ARW. With this setup, we obtain the room-temperature bias stability of 0.034 ± 0.01 deg/h and ARW of 3 ± 0.6 deg/sqrt(h) for all our homemade FOG sensors under a sensing data rate of 100 Hz, derived from the Allan deviation analysis as shown in Fig. 1b. Besides, the dynamic range of the sensor reaches >55 dB, covering the full linear response of

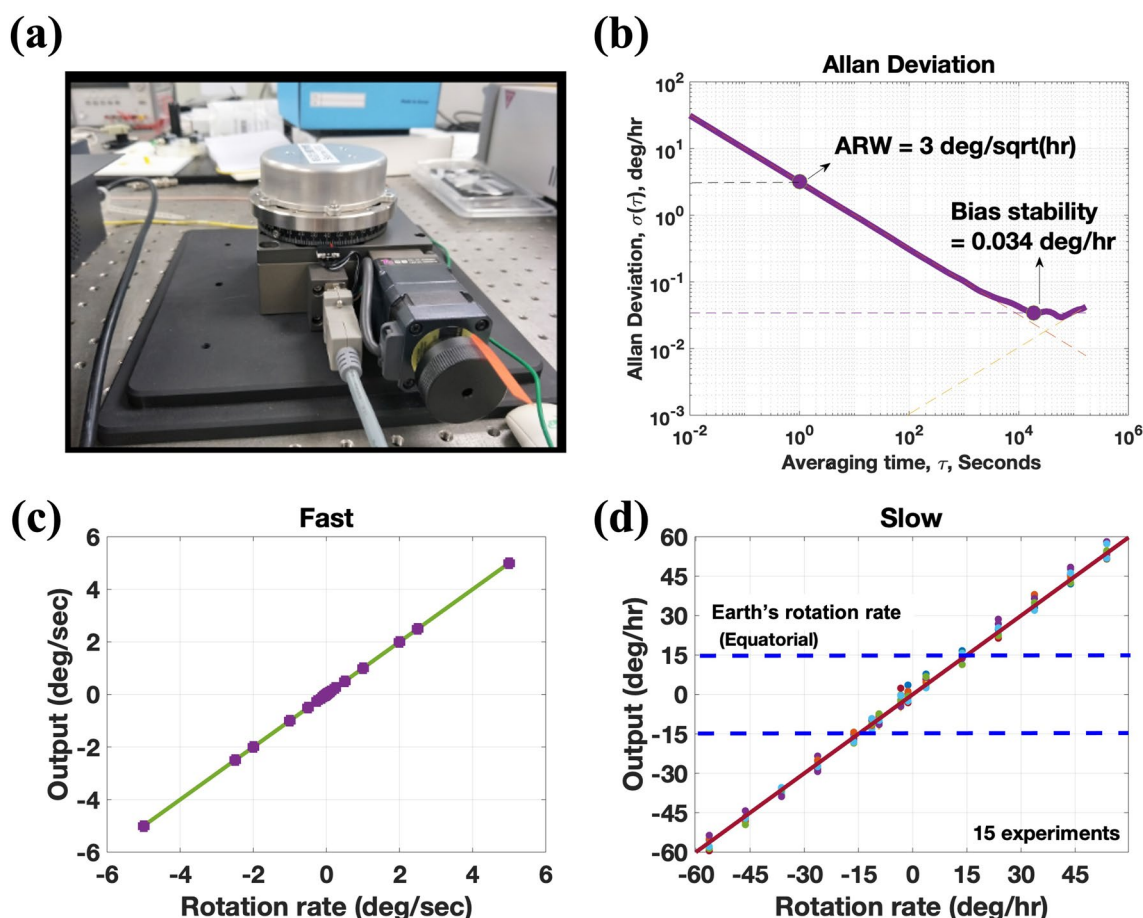


Fig. 1 **a** The physical picture of the NCU-FOG. **b** The Allan deviation analysis, which shows our FOG has a bias stability of 0.034 deg/h and an ARW of 3 deg/sqrt(h). **c** Relatively fast and **d** ultra-low rotational response characteristics, plotted with data from 15 independent measurements (represented by different colors). The solid lines shown in **c** and **d** are the fitted results with a linear scaling response.

the sensor from relatively fast to ultra-slow rotation rates, as shown in Fig. 1c and d. The rotation sensing of this sensor can be extended to -200 to $+200$ deg/s, and with the same linearity, this sensor can also provide the ultra-slow rotation sensing ability of <3.6 deg/h, which corresponds to 0.001 deg/s sensitivity. Figure 1d shows the statistics of 15 repeated measurements in an ultra-low rotation test environment, indicating the measurement results are highly repeatable and reliable. With a bias stability of ~ 0.034 deg/h, our FOG sensor can be of great potential for various vibration monitoring applications such as earthquake monitoring, track vibration monitoring, building, wind turbine, high-voltage electric tower, and carrier shaking monitoring, and heading detections, showing its greatly versatile applicability.

3 Observation and analysis

On 10 December 2020 at 21:19:58 Local Time (LT), a submarine M6.6 earthquake occurred near offshore Yilan, the epicenter 24.74° N 122.03° E with 75.7 km depth, reported by the Central Weather Bureau (CWB) of Taiwan (CWB 2020). NCU campus is located in Zhongli, the north-west of Taiwan (121.190733° N, 24.969367° E), which is 88 km away from the epicenter (as Fig. 2a shown). According to the report, the detected seismic intensity scale in Zhongli is 4 (Moderate). About 5 h later, an aftershock occurred at 02:15:08 LT on 11 December 2020 at the location of 24.53° N 121.97° E in 62.7 km depth with a magnitude $M_L = 5.7$ (from CWB). These two events are well recorded by NCU-FOG under the free-running passive measurement over the 14-h monitoring experiment conducted from 18:30:00 LT 10 December 2020 to 08:30:00 LT 11 December 2020.

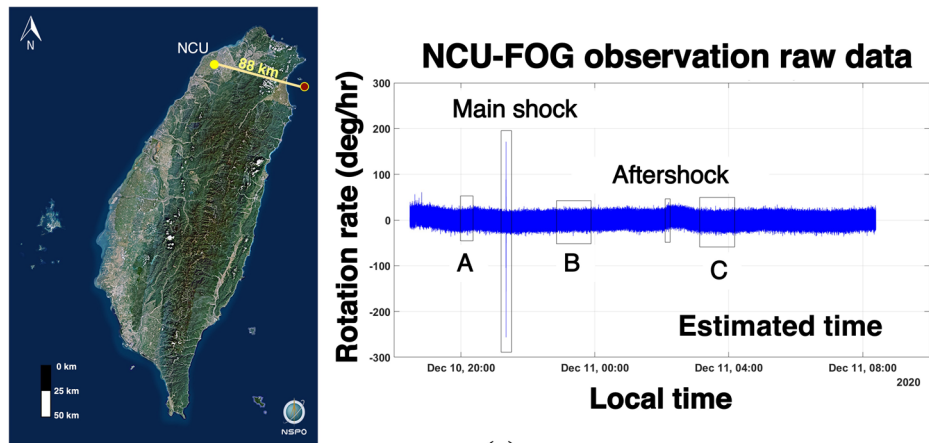
There were another two minor aftershocks ($M_L \sim 4$) of seismic intensity scale 1 (measured in Zhongli), occurring around 8 min and 4 h later than the main shock event, respectively, during the experiment period according to the CWB's report. However, these much weaker events were not detected by our FOG sensor with a sensing ability of <3.6 deg/h (or $\sim 10^{-5}$ rad/s) for rotational motions. According to the study by Zhou et al. (2019), we estimate this sensing ability of FOG can only detect an earthquake with a magnitude $>4-5$. This agrees with what we have observed for events with a magnitude >5 (i.e., the M6.6 main shock with intensity scale 4 and M5.7 aftershock with intensity scale 3) with our homemade FOG installed in NCU, Zhongli.

Figure 2a shows the 14-h unfiltered monitoring raw data of the seismic waves of the M6.6 Yilan earthquake event detected by the NCU-FOG sensor. Figures 2b and c show the FOG response of the rational component of the seismic waves during the main shock and aftershock periods, respectively. To study the data in the frequency

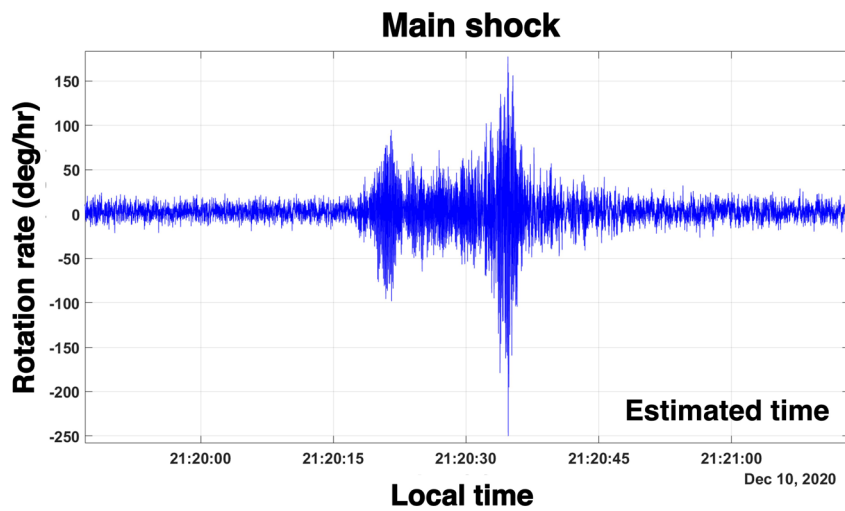
domain, we use the fast Fourier transform (FFT) algorithm to analyze the recorded FOG raw signal and the recorded raw data from a local seismograph (SMART 24A, located at 121.1849° N, 24.9679° E) during the main shock and M5.7 aftershock events (referring to the time periods marked as "Main shock" and "Aftershock" in Fig. 2a) as shown in Figs. 3 and 4, respectively.

We choose three time periods (marked as A, B and C in Fig. 2a) where signal exhibits relatively low fluctuations as the FOG signal background reference. These periods are well outside the time durations of the main shock and the three sensible aftershocks with intensity scales ≥ 1 according to the CWB's report. We found two observable frequency responses around 31 Hz and 38 Hz in the FFT spectrum of the time periods A, B and C, which corresponds to the inherent characteristic response of the FOG system. The insets of Figs. 3b–d and 4b–d show the seismograph recorded translational information with respect to the x-axis (North–South), y-axis (East–West), and z-axis (Perpendicular to the ground), which are titled as "Ses-X", "Ses-Y", and "Ses-Z", respectively. Some apparent DC offsets can be observed from these recorded waveforms, which can be attributable to the meter bias caused by some instrumental calibration issue. Actually, a DC offset of around 6.6 deg/h has also been observed from the FOG raw signals (see, e.g., Fig. 2c), which originates from the Earth's rotation rate measured at Zhongli, Taiwan. However, since all these DC offsets are observed to be relatively stable over time, they should only have a minor effect on the information we have processed and analyzed in this work. The results of the FFT analysis of the NCU-FOG and seismograph signals during the aftershock event are also shown in Fig. 4. It can be shown in Figs. 3 and 4, the major frequency response of the (rotational) signal from the FOG sensor is 11–13 Hz and 21–23 Hz for both the main shock and aftershock events, which is quite different from that analyzed with the seismograph data (translational information). The spectra of the seismograph FFT signals are mainly distributed in 1–5 Hz for X- and Y-axes, and <10 Hz for Z-axis. Similar spectral feature is also observed with the aftershock FFT data as shown in Fig. 4. Besides, from the FFT spectra shown in Figs. 3 and 4, it indicates the intensity of the main event is about half to one order of magnitude larger than that of the aftershock event for both the FOG and seismograph detection cases.

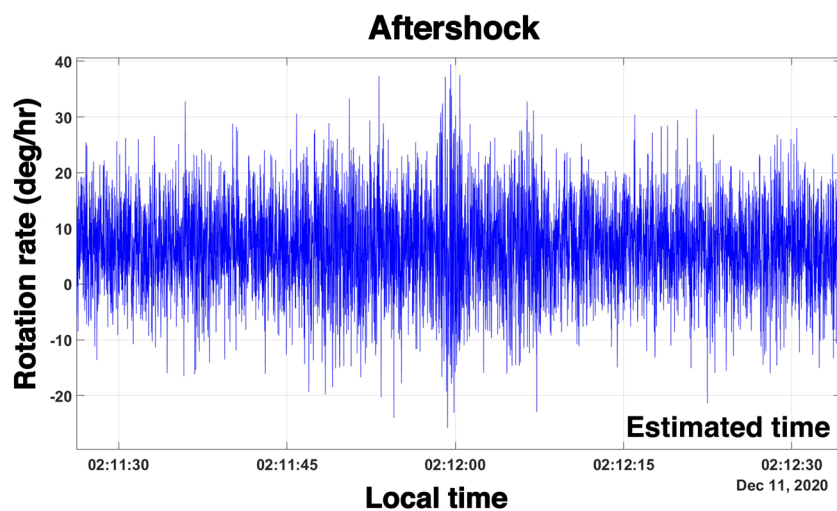
Unfortunately, the broadband seismograph (KS-200BH) at NCU was not functioning during the experiment period we performed for this study. To further confirm our analysis made above, we have accessed and studied the data recorded by nearest accessible broadband seismographs, Trillium240/Q330HR and Trillium 120 PH, located in Shibagianshan (the SBCB station of



(a)

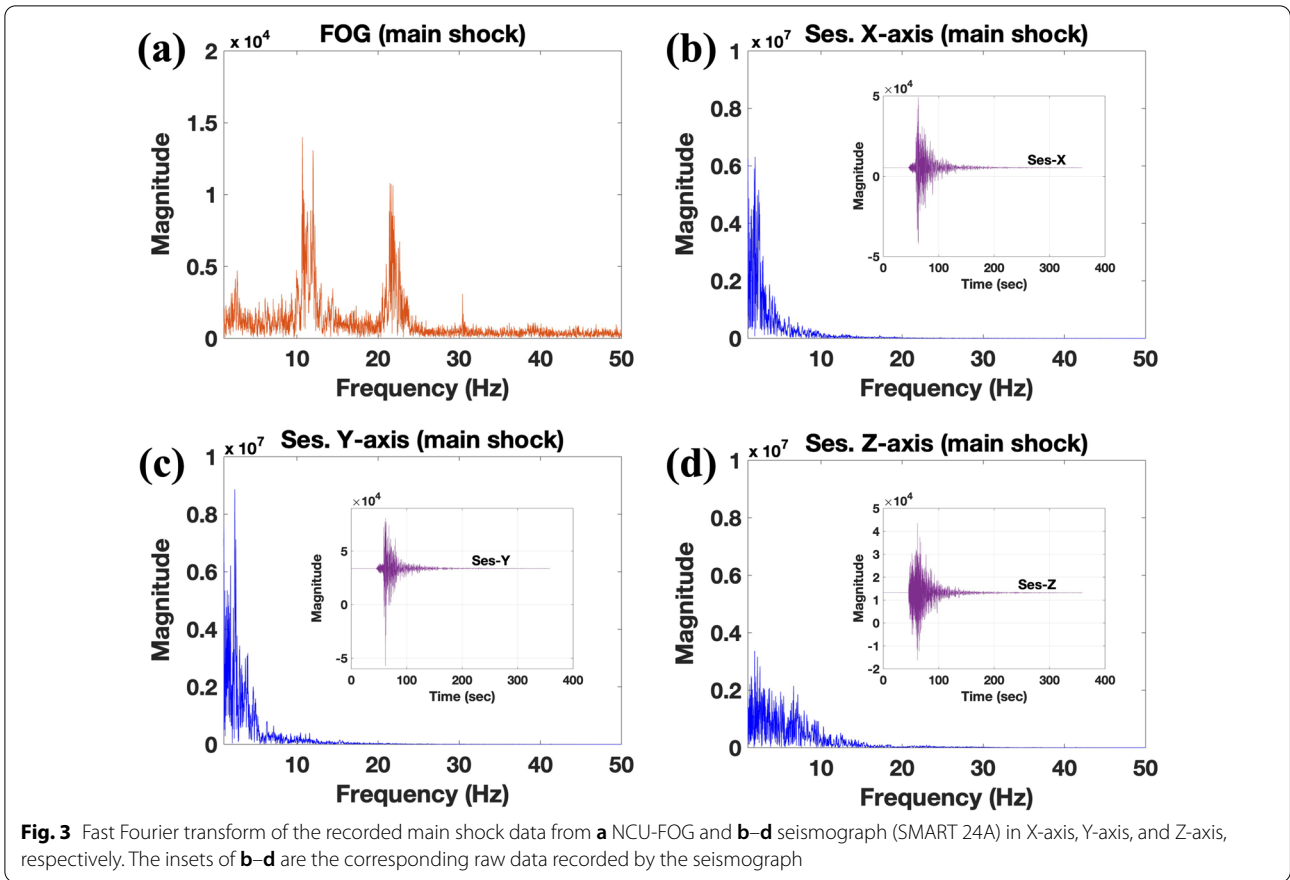


(b)



(c)

Fig. 2 **a** (Left) The seismic wave observation location (at NCU) with respect to the location of the M6.6 Yilan earthquake. (Right) 14-h unfiltered seismic-wave monitoring raw data with the NCU-FOG sensor. **b** and **c** FOG response of the rational component of the seismic waves monitored during the time periods of the main shock and the aftershock events, respectively.



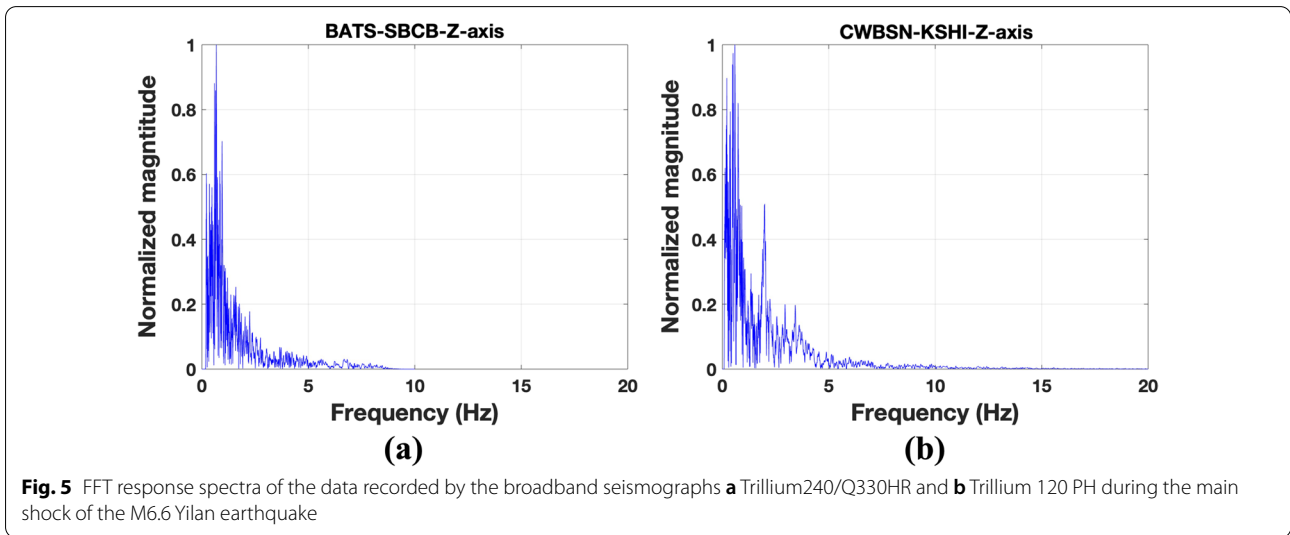
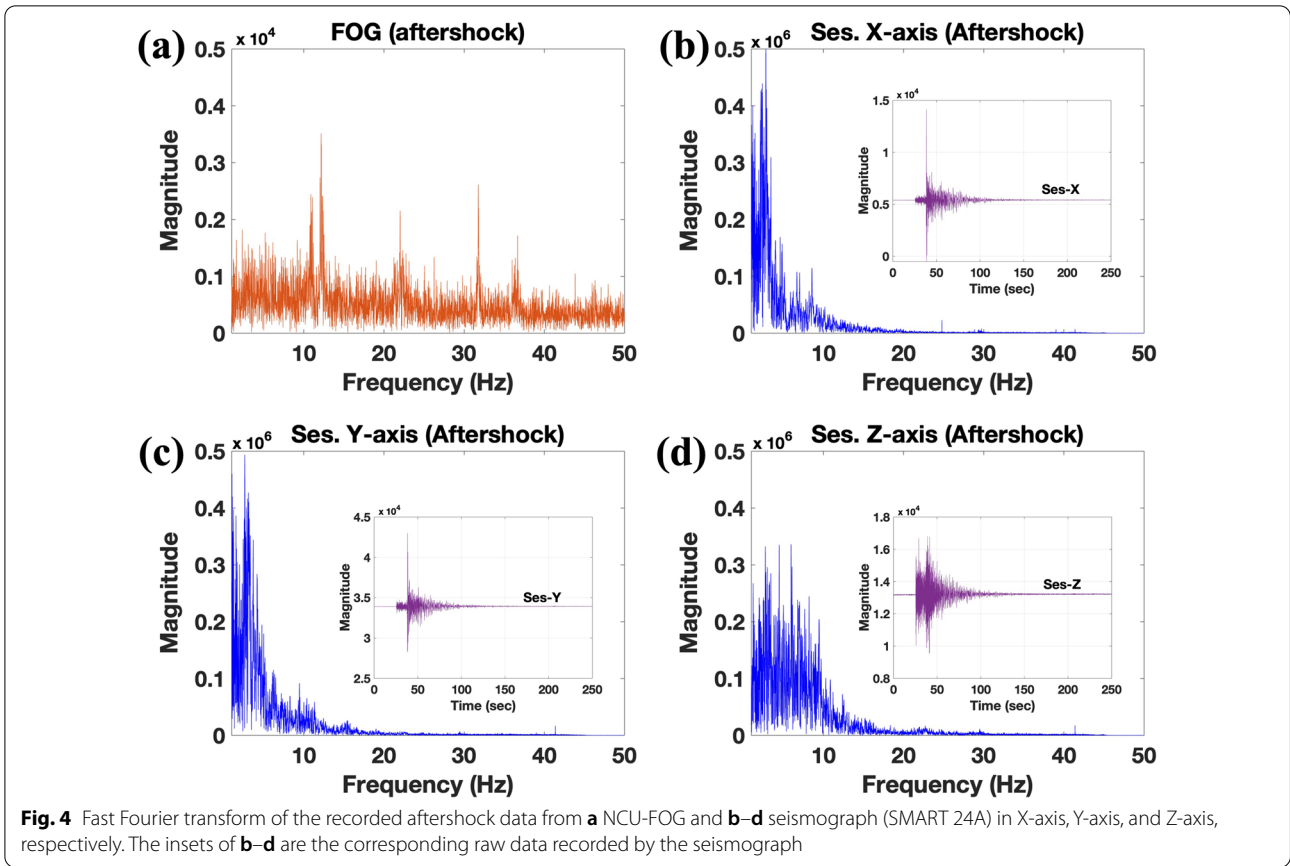
BATS) and Guansi (the KSHI station of CWBSN), Hsin-chu, respectively, during the period of the 2020 M6.6 Yilan earthquake. The SBCB and KSHI seismographs have a broader responsivity with bandwidths extended to 35 Hz and 150 Hz, respectively (the specifications of the two seismographs can be found in <https://www.passcal.nmt.edu/content/instrumentation/sensors/broad-band-sensors/t240-bb-sensor> and <https://www.nanometrics.ca/products/seismometers/trillium-120-posthole>, respectively). Figure 5a and b show the FFT response spectra of the data recorded by the two broadband seismographs, respectively, during the main shock of the earthquake event. It clearly shows the major frequency response of the seismographs to the shock waves was observed to fall within 0–10 Hz as that observed with the local seismograph (SMART 24A) studied above in Figs. 3 and 4, which could be attributed to the fast degraded (cut-off) sensitivity for a translational seismograph in a higher frequency range. The results also show FOG sensors can be an excellent seismometers complementary to widely-used translational seismographs as they can not only provide the missing rotation information but also respond more sensitively to high-frequency (rotational) motions in the seismic sensing technology.

4 Discussion and conclusion

In terms of the energy conservation, the sum of the strength of the signals detected by the FOG should be proportional to that detected by the seismograph, given by

$$\eta \sum_{t=0}^n \left(S_x^2(t) + S_y^2(t) + S_z^2(t) \right) = \xi \sum_{t=0}^n \left(A_{FOG}^2(t) \right), \tag{1}$$

where S_x , S_y , S_z , and A_{FOG} are the normalized amplitudes of the signals measured by the seismograph with respect to the x -axis, y -axis, and z -axis and by the FOG sensor, respectively, η and ξ are the proportional/scale factors. To investigate the temporal correlation of the shock waveforms of the translational and rotational components, we evaluate the correlation coefficients of the recorded seismograph and FOG data using five processing steps starting from the raw data (as shown in Fig. 6a and b), including Step 1: filtering out background noise and performing signal reconstruction, this is to apply FFT, digital (2–25 Hz) band-pass (BP) filtering, and then inversed-FFT signal processing to



(See figure on next page.)

Fig. 6 Raw data recorded by the FOG and seismograph sensors during the **a** main shock and **b** aftershock events. Resultant spectra and reconstructed signal waveforms generated in the signal processing Step 1 for the **c** main shock and **d** aftershock events. Normalized intensity of the seismic waves recorded by the seismograph and FOG sensors during the **e** main shock and **f** aftershock events under the energy conversion law (Eq. (1)). **g** Median-filtered main-shock and **h** aftershock signals recorded by the seismograph and FOG sensors

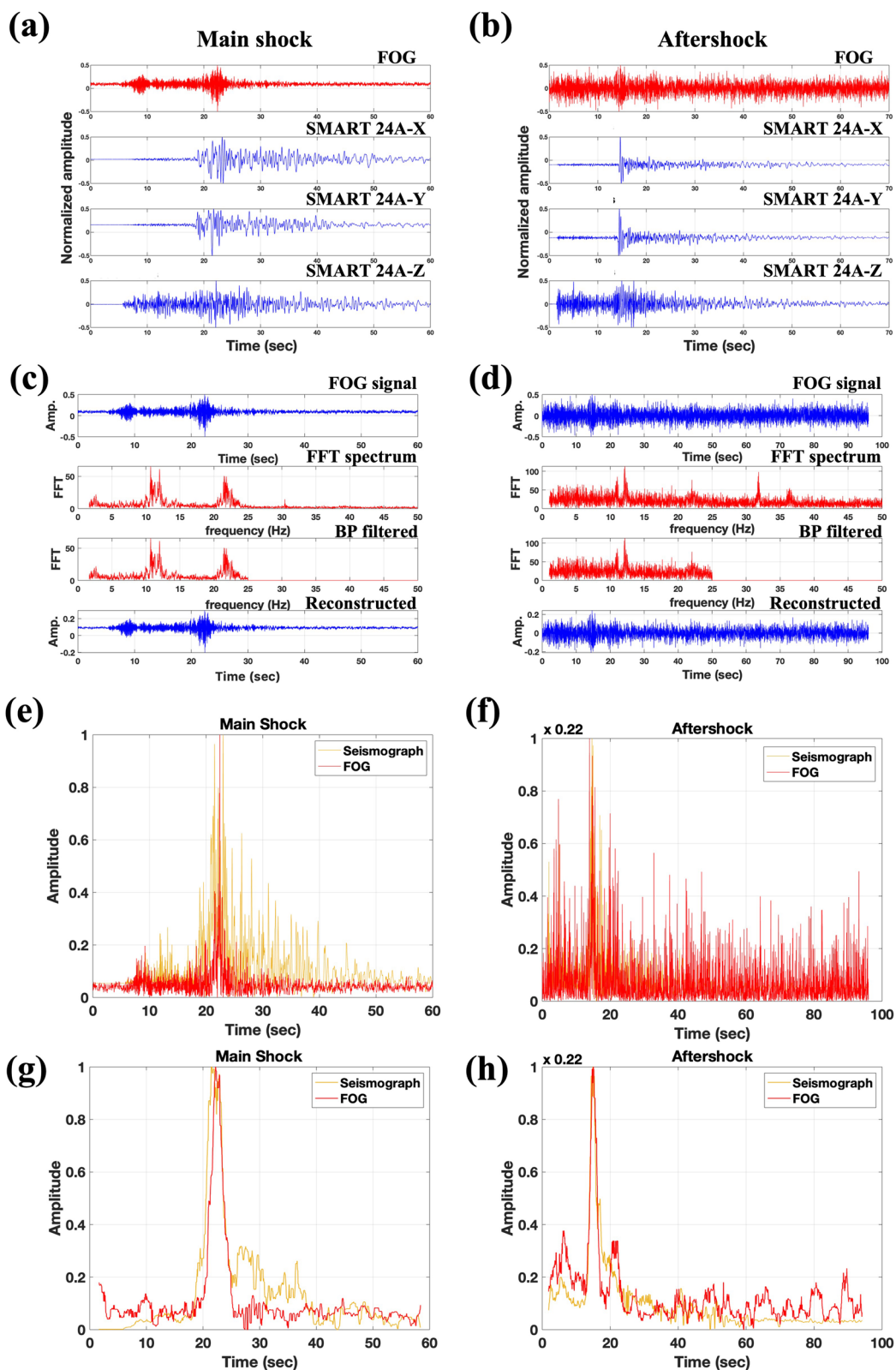


Fig. 6 (See legend on previous page.)

the raw data, the resultant spectra and reconstructed signal waveforms are shown in Fig. 6c and d. A 2–25 Hz BP filter is used to filter out the strong DC response (0–2 Hz) and those noises contributed from the characteristic eigenfrequencies (such as those around 31 and 38 Hz) of the FOG sensor, which helps to reconstruct a more authentic time-domain signals, Step 2: normalization of the translational and rotational signals based on the energy equality relationship given in Eq. (1), Step 3: synchronization of the seismograph and FOG signals for the temporal correlation evaluation, Step 4: applying the median filter to both the seismograph and FOG data with a proper filter time window between 1 and 5 s to best correlate the data of the two events, and Step 5: performing the main period sampling to mitigate the random noise, this is to choose a proper time window to help the processing of raw noisy signals into smoother waveforms without losing the information fidelity to facilitate the correlation calculation. Figure 6e and f show the resultant seismic waveforms after the Step 2 process for the seismograph and FOG data during the main shock and aftershock, respectively. Figure 6g and h show the main-shock and aftershock signals processed with the five processing steps for both the seismograph and FOG sensors, respectively, illustrating the wave forms detected by the two different sensors are significantly correlated. We found the application of a filter time window between 1 and 5 s can yield similar but around the optimum smooth filtering results as presented in Fig. 6g and h.

From Fig. 6g and h, it shows the main peaks of the signals recorded by the two different sensors are in great coincidence for both events. Some discrepancy in the sidelobes between the two signals could arise from the different sensitivity/responsivity of the two sensors to a relatively weak (sidelobe) signals. It can also be attributable to the different wave behavior exhibited between the rotational and translational components of a seismic wave. We found the correlation coefficients (Akoglu 2018) are >0.85 and >0.86 for the main-shock and aftershock wave signals detected by the two sensors, respectively, in a 60-s monitoring window, while the correlation coefficients are as high as 0.9064 and 0.8953 within the 10-s window of the main-shock and aftershock peak periods. The numerical evaluation of the correlation coefficients has been conducted based on the Pearson correlation coefficient formula (Press et al. 1992).

The information of the time-varying seismic-wave spectra of the main shock and aftershock events detected by the NCU-FOG can be analyzed by the short-time Fourier transform (STFT) method (Jarmolowski et al. 2021). Figure 7a–d show the time-dependent frequency distributions obtained from the STFT analysis made in the

time periods of the main shock, aftershock, duration A, and duration C (see Fig. 2a), respectively. We don't redundantly show the result for duration B as it has exhibited the same information as that presented from the results with durations A and C. The results shown in Fig. 7 basically agree with those we have observed and analyzed from the recorded data presented in previous sections, revealing the major frequency components of the main shock and aftershock waves are distributed in 11–13 Hz and 21–23 Hz, while relatively weak responses around 31 Hz and 38 Hz are found to be the system characteristic frequency components. To further investigate the noise spectrum detected by the FOG sensor during a relatively stable background condition (such as duration A, B, or C), a FFT of the signals recorded by our FOG operating at a 100-Hz data rate over a period of time (1.5 h) under a normal but calm/stable environment has been conducted, as shown in Fig. 7e. The result clearly shows the FOG can provide a detection limit (or responsivity) for a (rotational) motion signal with an amplitude well below -20 dB (with respect to the DC level) from a lower frequency range to <-30 dB at a higher frequency. Two prominent signals at 31 and 38 Hz emerging from the frequency response curve originate from the system eigenfrequencies as discussed above. According to the above analysis, we can present more authentic information of the FOG recorded seismic-wave signals by excluding those system characteristic frequencies from the raw data shown in Fig. 2. Figure 8 shows the rotation rate information of the seismic waves after applying a filter with a band-pass window between 2 and 25 Hz during the 14-h observation of the main shock and aftershock events by the NCU-FOG sensor. By comparing the results between the unfiltered data shown in Fig. 2 and the filtered data shown in Fig. 8, we found the angular noise level has been remarkably reduced from $\sim \pm 20$ deg/h with the unfiltered raw data to $\sim \pm 10$ deg/h with the 2–25 Hz BP filtered data, leading to an improved signal-to-noise ratio by a ~ 3 -dB enhancement.

FOG is a highly sensitive optical sensor based on the light interference effect associated with the wave phase shift even it is subtle. In particular, FOGs can precisely detect the rotational rate information of a moving object and respond more sensitively to high-frequency vibrations/shocks, in which FOGs could have a great potential of ability to detect the information of the rotational component of micro-shock waves prior to the main shock in an earthquake event. FOGs can thus be promisingly utilized to deploy a sensing network in the earthquake frequent areas to increase the possibility of earthquake early warning (Peng et al. 2019). Before this, it is practically important to develop a calibration system to accurately test the frequency response of the

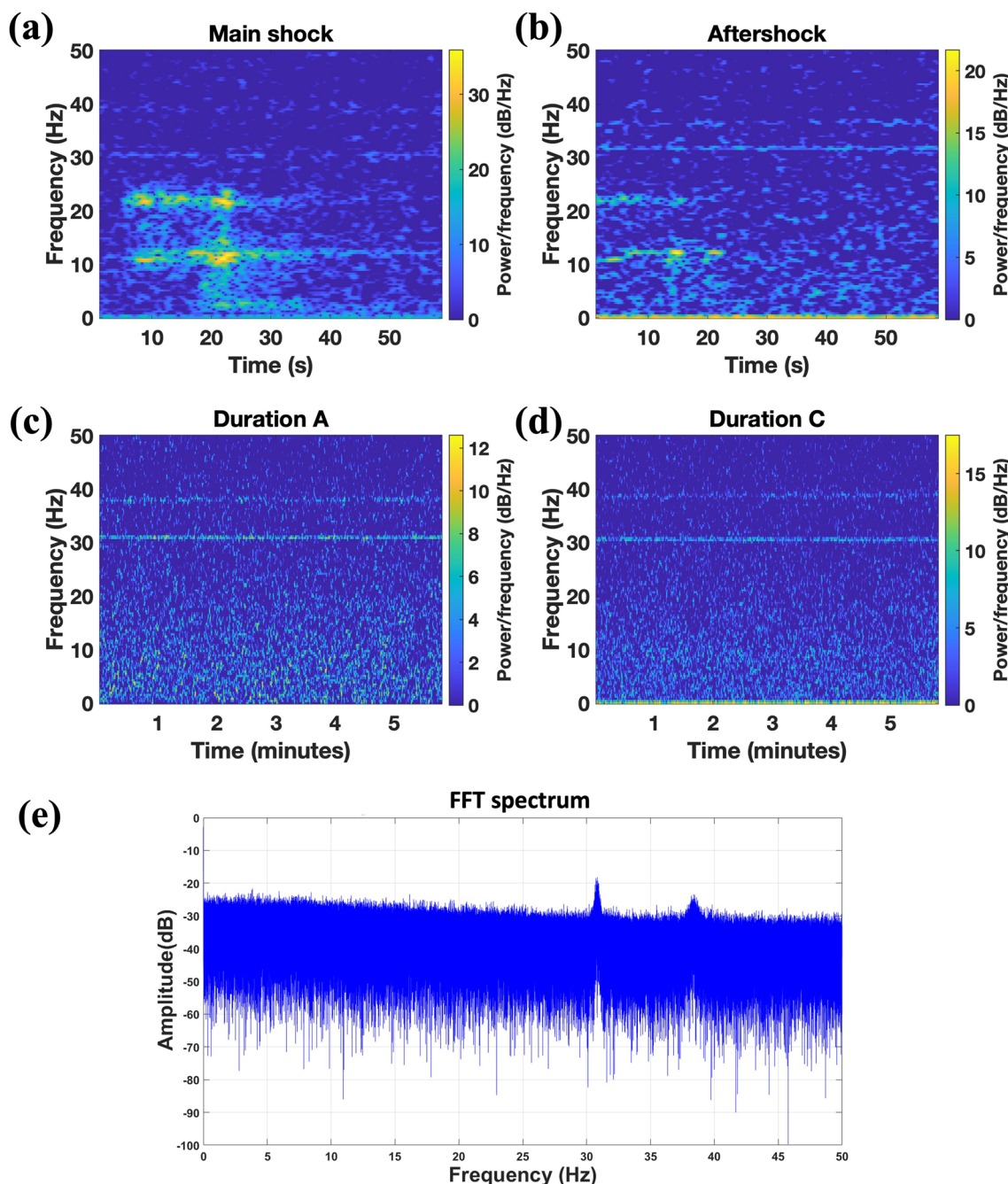


Fig. 7 Time-dependent frequency distributions obtained from the STFT analysis made in the time periods of the **a** main shock, **b** aftershock, **c** duration A, and **d** duration C. **e** FFT spectrum obtained from signals recorded by our FOG operating at a 100-Hz data rate over a period of time under a normal but calm/stable environment

FOG, and obtain sensitivity and linearity, in order to meet the specifications of seismology. Besides, more examinations for FOG in the future are also required for the further investigation of key issues such as the understanding of the dynamic response of a site under

the action of far-field and near-field shockwaves or even other disturbance like typhoon.

Besides seismic wave detections, FOG sensors are also of great advantage to many other applications such as the vibration monitoring of volcanos, wind turbines, wafer isolation platform, high tension towers, buildings, and

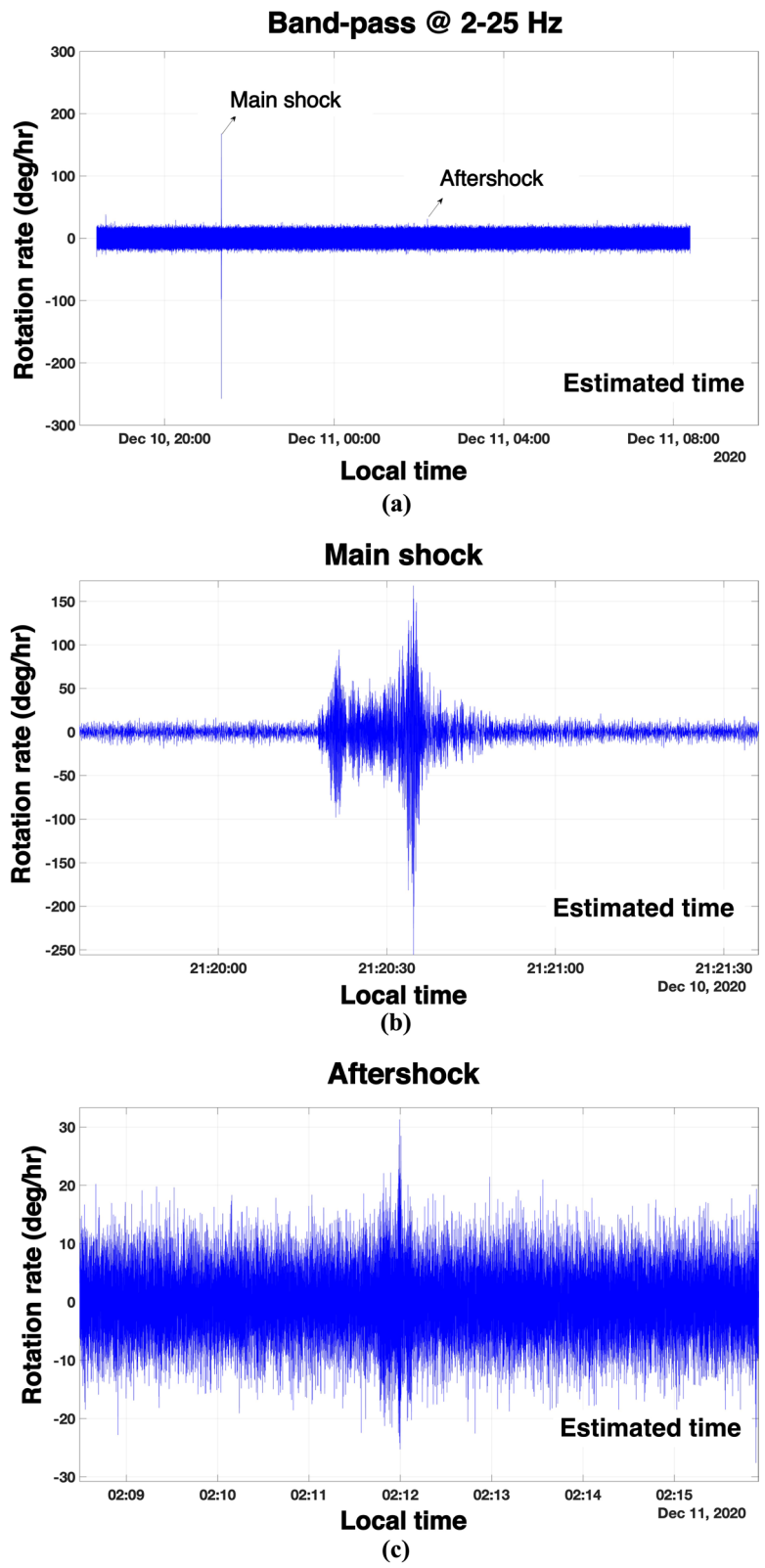


Fig. 8 5–30 Hz band-pass filtered rotation rate information of the seismic waves recorded during the **a** 14-h, **b** main-shock, and **c** aftershock time periods

vehicle bodies. We believe such a high precision, compact and robust all-solid FOG seismometer provides an exceptional solution for dynamic rotational sensing applications. Based on this technology, we expect to build a powerful seismometer featuring a six degree-of-freedom observation array (Specifically in each constituent sensor unit, we will need 3 gyroscopes (FOGs) and 3 accelerometers installed in the three orthogonal axes (each with one gyroscope and accelerometer) of a user defined Cartesian coordinate system to obtain all the independent, six-degree-of-freedom (Rx, Ry, Rz, Ax, Ay, Az) motion components simultaneously). Further information of modeling and measuring rotational motion components induced by earthquake can be found in (Zhou et al. 2019; Jaroszewicz et al. 2016) to expedite the advances of the earthquake science and technology.

In the future, applications such as the comparison of array rotation with single-point rotation, the tilt correction of the horizontal component of the seismometer, the understanding of the focal mechanism, and the phase identification of seismic waves will all be the interesting and critical topics to study.

Acknowledgements

This work was financially supported by the Center for Astronautical Physics and Engineering (CAPE) from the Featured Area Research Center program within the framework of Higher Education Sprout Project by the Ministry of Education (MOE) in Taiwan. This study is supported by the Taiwan Ministry of Science and Technology (MOST) grants MOST 110-2823-8-008-004- from TRISTU office of department of Academia-Industry Collaboration and Science Park Affairs, MOST 110-2627-M-008-001, MOST 111-2119-M-008-002, MOST 110-2923-E-008-001, and MOST 110-2823-8-008-005. The authors thank the Taiwan Semiconductor Research Institute (TSRI), Taiwan and the Nano Facility Center at National Yang Ming Chiao Tung University, Taiwan for the support of the device microfabrication (MOST 110-2731-M-009-001). The authors thank to the data owner which seismic data used in this paper was provided from the Professor Yen's Lab.

Author contributions

H. P. C., Y. H. C., and C. C. C. designed the fully homemade, compact FOG sensors, H. P. C., S. H. C., C. L. H., and H. Y. constructed the NCU-FOG sensors and conducted the seismic monitoring experiments, J. Y. L., H. Y. Y., H. P. C., C. C. C., and Y. H. C. studied and analyzed the measured seismic-wave data, H. P. C. drafted the manuscript, Y. H. C., J. Y. L., C. C. C., and H. Y. Y. revised the manuscript. All authors read and approved the final manuscript.

Funding

Ministry of Education, the Center for Astronautical Physics, Jann-Yenq Liu, Engineering (CAPE), Jann-Yenq Liu, Ministry of Science and Technology, Taiwan, MOST 110-2823-8-008-004-, Chii-Chang Chen, 110-2627-M-008-001, Yen-Hung Chen, 110-2923-E-008-001, Yen-Hung Chen.

Availability of data and material

All data generated or analysed during this study are included in this published article.

Declarations

Competing interests

The authors declare that they do not have any competing interests.

Author details

¹Center for Astronautical Physics and Engineering, National Central University, Taoyuan City, Taiwan. ²Department of Optics and Photonics, National Central University, Taoyuan City, Taiwan. ³Polaris Photonics Limited, Taipei City, Taiwan. ⁴Department of Space Science and Engineering, National Central University, Taoyuan City, Taiwan. ⁵Center for Space and Remote Sensing Research, National Central University, Taoyuan City, Taiwan. ⁶Department of Earth Sciences, National Central University, Taoyuan City, Taiwan.

Received: 18 January 2022 Accepted: 20 December 2022

Published online: 30 December 2022

References

- Akoglu H (2018) User's guide to correlation coefficients. *Turk J Emerg Med* 18(3):91–93
- Arditty HJ, Lefevre HC (1981) Sagnac effect in fiber gyroscopes. *Opt Lett* 6(8):401–403
- Cao Y et al (2021) The development of a new IFOG-based 3C rotational seismometer. *Sensors* 21(11):3899
- Fiber Optic Gyroscope Market (2021) Fiber Optic Gyroscope Market Analysis, By Sensing Axis (1-Axis, 2-Axis, 3-Axis), By Device Type (Gyrocompass, Inertial Measurement Unit), By Vertical (Automotive, Robotics, Mining, Healthcare), and Region - Global Market Insights 2022 to 2032 (Fact. MR). <http://www.factmr.com/report/2187/fiber-optic-gyroscope-market>
- Jaroszewicz L, Kurzych A, Krajewski Z, Marc P, Kowalski J, Bobra P, Zembaty Z, Sakowicz B, Jankowski R (2016) Review of the usefulness of various rotational seismometers with laboratory results of fibre-optic ones tested for engineering applications. *Sensors* 16(12):2161
- Jarmolowski W, Wielgosz P, Krypiak-Gregorczyk A, Milanowska B, Haagmans R (2021) Seismic ionospheric disturbances related to Chile-Illapel 2015 earthquake and tsunami observed by Swarm and ground GNSS stations. vEGU21, the 23rd EGU General Assembly, held online 19–30 April, 2021, id.EGU21-8218. <https://doi.org/10.5194/egusphere-egu21-8218>
- Kurosu S, Yamada J, Tomizawa H (1979) Seismometer using gyroscope measurement of vertical seismic motion. *Trans Soc Instrum Control Eng* 15(1):83–88
- Lee WHK, Huang BS, Langston CA, Lin CJ, Liu CC, Shin TC, Teng TL, Wu CF (2009) Progress in rotational ground-motion observations from explosions and local earthquakes in Taiwan. *Bull Seismol Soc Am* 99(2B):958–967. <https://doi.org/10.1785/0120080205>
- Lee W, Evans JR, Huang BS et al (2012) Measuring rotational ground motions in seismological practice. In *New manual of seismological observatory practice 2 (NMSOP-2)* 1–27.
- Lefevre HC (2014) *The fiber-optic gyroscope*. Artech house. 25 pp
- Lin CJ, Liu CC, Lee WH (2009) Recording rotational and translational ground motions of two TAIGER explosions in northeastern Taiwan on 4 March 2008. *Bull Seismol Soc Am* 99(2B):1237–1250
- Lough AC (2014) *Studies of seismic sources in Antarctica using an extensive deployment of broadband seismographs*. Washington University, St. Louis
- Peng C et al (2019) Performance evaluation of a dense MEMS-based seismic sensor array deployed in the Sichuan-Yunnan border region for earthquake early warning. *Micromachines* 10:11
- Press WH, et al. (1992) *Numerical recipes in C: diskettes IBM 3 1/2" for IBM PC, PS/2, DOS*. Cambridge Univ. Press
- Simonelli A et al (2018) Rotational motions from the 2016, Central Italy seismic sequence, as observed by an underground ring laser gyroscope. *Geophys J Int* 214(1):705–715
- Simonelli A et al (2021) Monitoring local earthquakes in central Italy using 4C single station data. *Sensors* 21(13):4297
- Hees V, Vincent T et al (2009) Reproducibility of a triaxial seismic accelerometer (DynaPort). *Med Sci Sports Exerc* 41(4):810–817
- Velikoseltsev A et al (2012) On the application of fiber optic gyroscopes for detection of seismic rotations. *J Seismol* 16(4):623–637
- Warner D (2014) Maurice Ewing, Frank Press, and the long-period seismographs at Lamont and Caltech. *Earth Sci Hist* 33(2):333–345
- Yuan S, Simonelli A, Lin CJ et al (2020) Six degree-of-freedom broadband ground-motion observations with portable sensors: validation, local earthquakes, and signal processing. *Bull Seismol Soc Am* 110(3):953–969

Zhou C et al (2019) Rotational motions of the Ms7.0 Jiuzhaigou earthquake with ground tilt data. *Sci China Earth Sci* 62(5):832–842

Publisher's Note

Springer Nature remains neutral with regard to jurisdictional claims in published maps and institutional affiliations.

Submit your manuscript to a SpringerOpen[®] journal and benefit from:

- ▶ Convenient online submission
- ▶ Rigorous peer review
- ▶ Open access: articles freely available online
- ▶ High visibility within the field
- ▶ Retaining the copyright to your article

Submit your next manuscript at ▶ [springeropen.com](https://www.springeropen.com)
